Phase Behavior and Stabilization of Microgel Arrays

Gang Huang† and Zhibing Hu*

Departments of Chemistry and Physics, University of North Texas, Denton, Texas 76203

Received January 29, 2007; Revised Manuscript Received March 12, 2007

ABSTRACT: Monodispersed copolymer *N*-isopropylacrylamide and allylamine (PNIPAM-*co*-allylamine) colloidal spheres with various cross-linking densities have been synthesized using precipitation polymerization. The phase behavior of dispersions of these microgels has been investigated as functions of polymer concentration, temperature, and cross-linking density. It has been found that such dispersions exhibit liquid, crystal, and glass phases. For the particles with the cross-linker to monomer ratio around 1.5 mol % at 21 °C, colloidal crystals have been observed in polymer concentrations ranging from 1.0 to 3 wt %. As this ratio increases, colloids form crystals in higher concentrations. Following the phase diagram, a new route to make a crystalline structure with a high polymer concentration has been obtained by initiating crystallization near the crystal formation temperature but stabilizing the crystalline structure below the glass transition temperature. The gelation is achieved by bonding the PNIPAM-*co*-allylamine spheres using glutaric dialdehyde as a cross-linker at room temperature under a neutral pH. The hydrogel with a higher polymer concentration has a better mechanical strength, while a mild synthesis condition at pH 7 makes this material particularly useful for biomedical applications, including loading biomolecules between the particles for controlled drug delivery. The iridescent patterns of these crystalline hydrogels are tunable in response to external stimuli. UV−vis spectroscopy has been used to monitor the change of the Bragg diffraction from these hydrogels as a function of temperature, pH, and protein concentration.

Introduction

Hydrogels are water-based polymer networks that can be designed to expand and contract in response to various external stimuli.[1] They have been used as models for fundamental investigations in phase transitions[1,2] and for applications in biomaterials[3] and controlled drug delivery.[4−7] When hydrogels are made as monodisperse nano- or microspheres, they can self-assemble into colloidal arrays,[8−15] similar to hard spheres.[16−19] Recently, hydrogels with periodic structures have been intensively investigated.[20−24] This is because the lattice spacing of such a structure is of the order of hundreds of nanometers, therefore interacting strongly with visible light, leading to environmentally tunable optical Bragg diffraction.[20] Specifically, Asher and co-workers used a three-dimensional crystalline colloidal array (CCA) of monodisperse, highly charged polystyrene latex particles to polymerize within a hydrogel.[20] The volume phase transition of the hydrogel causes the change in the CCA lattice spacing, resulting in the shift of the diffracted wavelength of light. Inverse opal hydrogels have been also developed by polymerization of a hydrogel within the interstitial space of a colloidal crystal template either with polystyrene or with silica, followed by removing the template.[21,22] By incorporating different functional groups, these gels have been used as glucose or pH sensors.[21,22] Our group has proposed to synthesize bulk hydrogels by covalently bonding self-assembled microgels.[23] The covalent bonding contributes to structural stability, while self-assembly provides the gel with crystal structures that diffract light, resulting in colors. Such stable periodic 3D structures allow us to obtain useful functionality not only from the constituent gel building blocks but also from the long-range ordering that characterizes these structures.[19]

Here we present a complete report on the formation of mesoscopical crystalline hydrogels with high mechanical strength using the heating−cooling process following a recent communication.[24] We will first discuss synthesis of PNIPAM microgels functionalized with allylamine group and with different cross-linking densities. Then we show the phase behavior of aqueous dispersions of these microgels. Changing the degree of cross-linking can vary the hardness and regularity of the particles and has been shown to affect viscoelastic properties of microgel dispersions.[25] Our results demonstrate that cross-linking density also plays a key role for the formation of microgel colloidal crystals, in addition to factors of temperature and polymer concentration. Following the phase diagram, crystalline hydrogels with high polymer concentration have been obtained by initiating the crystallization process near the colloidal crystal melting temperature while subsequently covalently bonding these microgels below the glass transition temperature. This is taking the advantage that the thermally sensitive microgels in colloidal glasses can be converted into ordered crystals via the particle-based volume transition as reported by Lyon and co-workers.[26] The shear modulus of the crystalline hydrogels has been determined. Bragg diffraction from these gels has been studied using a UV−vis spectrometer under various external stimuli including temperature, pH, and bovine serum albumin (BSA) concentration. This new class of hydrogel opals with high mechanical strength has a potential in applications for chemical and biological sensors, optical switching, and controlled drug delivery.

Experimental Section

Materials. *N*-Isopropylacrylamide (NIPAM) was bought from Polyscience Co. and used as received. Cross-linking agent *N*,*N*′-methylenebis(acrylamide) (BIS) was purchased from Bio-Rad Co. Potassium persulfate (KPS), sodium dodecyl sulfate (SDS), glutaric dialdehyde, and allylamine were purchased from Aldrich Chemical Co.

Synthesis of PNIPAM-*co*-allylamine Microgels. PNIPAM-*co*-allylamine microgels were synthesized using a precipitation polymerization method.[27] 3.845 g of NIPAM monomer, 0.2 g (10% molar ratio) of allylamine monomer, a certain amount of methyl-

* Corresponding author. E-mail: zbhu@unt.edu.
† Current address: Bioengineering Department, University of Utah, Salt Lake City, UT 84112.

10.1021/ma070253d CCC: $37.00
Published on Web 04/19/2007

Table 1. Compositions of Five Batches of Pregel Solutions

batch	NIPAM (g/mL)	Bis (g/mL)	Bis/NIPAM (mol %)	KPS (g/mL)	SDS (g/mL)	R_h (nm)
1	0.015 38	6.29×10^{-4}	3.0	6.2×10^{-4}	3.016×10^{-4}	125
2	0.015 38	5.26×10^{-4}	2.5	6.2×10^{-4}	3.022×10^{-4}	123
3	0.015 38	4.19×10^{-4}	2.0	6.2×10^{-4}	3.024×10^{-4}	130
4	0.015 38	3.14×10^{-4}	1.5	6.2×10^{-4}	3.078×10^{-4}	126
5	0.015 38	5.26×10^{-4}	2.5	6.2×10^{-4}	3.020×10^{-4}	140

enebis(acrylamide) (BIS) as cross-linker, sodium dodecyl sulfate as surfactant, and 230 mL of deionized water were mixed in a reactor. The solution was heated up to 60 °C under nitrogen bubbling for about 40 min. 0.155 g of potassium persulfate dissolved in 20 mL of deionized water was added to initiate the reaction. The reaction was carried out at 60 °C for 5 h. After cooling the solution to room temperature, the final reaction dispersion was exhaustively dialyzed in a dialysis tube for 7 days while the deionized water (conductivity $< 1\ \mu S\ cm^{-1}$) outside the tube was changed three times a day.

Four batches of PNIPAM-*co*-allylamine microgels were synthesized with the mole ratios of cross-linking agent, BIS, to NIPAM monomer ranging from 0.015 to 0.03. Their compositions of prereaction solutions and hydrodynamic radii are shown in Table 1. The microgels of batch 5, prepared for the previous study,[24] had the same BIS/NIPAM ratio as that in batch 2 but a slightly higher particle radius.

Synthesis of Crystalline Hydrogels. The dispersions of PNIPAM-*co*-allylamine microgels taken out from dialysis tubes were further cleaned and concentrated using an ultracentrifuge with a speed of 40 000 rpm for 2 h. These dispersions were then adjusted to different polymer concentrations at 21−23 °C and were heated from 23 to 40 °C and then cooled back to 23 °C with a rate about 0.4 °C/min. After observing crystalline structures, glutaric dialdehyde (0.04 g of 25 wt % for 1 g dispersion) as a cross-linker was added to the top of the dispersion. This chemical agent diffused through the dispersion and covalently bonded the particles together in neutral pH. Here allylamine offered the free amine function groups on the surface of the microgels for cross-linking. The particle assembly with a crystalline structure was stabilized by the cross-linking reaction for about 2 days and removed from the test tube by injecting water to the bottom of the tube using a syringe.

Laser Light Scattering Characterization. A laser light scattering (LLS) spectrometer (ALV, Germany) equipped with an ALV-5000 digital time correlator was used with a helium−neon laser (Uniphase 1145P, output power of 22 mW and wavelength of 632.8 nm) as the light source. The incident light was vertically polarized with respect to the scattering plane, and the light intensity was regulated with a beam attenuator (Newport M-925B). The scattered light was conducted through a thin (~100 μm in diameter) optic fiber leading to an active quenched avalanche photodiode (APD), the detector.

In static light scattering (SLS), the angular dependence of the excess Rayleigh ratio $R_{vv}(q)$ of dilute polymer solutions or nanoparticle dispersions is measured. $R_{vv}(q)$ is related to the weight-average molar mass M_w, the second virial coefficient A_2, and the *z*-average root-mean-square radius of gyration $\langle R_g^2\rangle_z^{1/2}$ (or simply $\langle R_g\rangle$) by[28]

$$\frac{KC}{R_{vv}(q)} \cong \frac{1}{M_w}\left(1 + \frac{1}{3}\langle R_g^2\rangle q^2\right) + 2A_2C \qquad (1)$$

where $K = 4\pi^2 n^2 (dn/dC)^2/(N_A\lambda_0^4)$ and $q = (4\pi n/\lambda_0)\sin(\theta/2)$ with N_A, n, C, λ_0, and θ being Avogadro's constant, the solvent refractive index, the solid concentration (g/cm^3 or g/g), the light wavelength in the vacuum, and the scattering angle, respectively. In SLS, the samples were scanned from angle 30° to 120° with a 5° interval. With the same dilute samples, we could perform DLS and SLS measurements in turns.

The relation of interest in dynamic light scattering is the fluctuation of the scattered intensity with time *t*. The intensity−intensity time correlation function $G^{(2)}(t,q)$ in the self-beating mode can be expressed by[28,29]

$$G^{(2)}(t,q) = \langle I(t,q)\, I(q,0)\rangle = A[1 + \beta|g^{(1)}(t,q)|^2] \qquad (2)$$

where t is the delay time, A is measured baseline, and β is the coherence factor. For a polydispersed sample, $|g^{(1)}(t,q)|$ is the first-order electric field time correlation function $E(t,q)$ and is related to the line-width distribution $G(\Gamma)$ by

$$g^{(1)}(t,q) = \langle E(t,q)\, E^*(0,q)\rangle = \int_0^\infty G(\Gamma)e^{-\Gamma\tau}\, d\Gamma \qquad (3)$$

$G(\Gamma)$ can be calculated from the Laplace inversion of $g^{(1)}(t,q)$. $g^{(1)}(t,q)$ was analyzed by a cumulant analysis to get the average line width $\langle\Gamma\rangle$ and the relative distribution width $\mu_2/\langle\Gamma\rangle^2$. The extrapolation of Γ/q^2 to $q \to 0$ led to the translational diffusion coefficient (D). This corresponding analysis of this function yields the diffusion coefficient D, which can be translated into the hydrodynamic radius R_h by the Stokes−Einstein relation:

$$R_h = k_B T/6\pi\eta D \qquad (4)$$

where k_B, η, and T are the Boltzmann constant, the solvent viscosity, and the absolute temperature, respectively. The DLS measurements were carried out at $\theta = 60°$.

UV−Vis Characterization. The polymer concentration of a microgel dispersion was obtained by completely drying the dispersion at 60 °C and then weighing it. The turbidity of the PNIPAM-*co*-allylamine microgel dispersions was measured as a function of wavelength using a UV−vis spectrophotometer (Agilent 8453).

Results and Discussion

1. Light Scattering Characterization of PNIPAM-*co*-allylamine Microgels. Figure 1a shows hydrodynamic radius distributions of PNIPAM-*co*-allylamine particles (batch 2) with cross-linking density about 2.5 mol % in a dilute dispersion at 23 and 35 °C, respectively. At 23 °C, the microgels are in their swollen state and have the average hydrodynamic radius about 123 nm. At 35 °C, the radius of microgels reduces to about 70.3 nm. The temperature dependence of the hydrodynamic radius for PNIPAM-*co*-allylamine microgels (batch 5) is shown as Figure 1b. The radius of the PNIPAM microgels without allylamine, prepared using the same conditions as PNIPAM-*co*-allylamine, is also included in Figure 1b for comparison. The temperature at which the derivative of the radius vs temperature curve reaches a maximum value is usually defined as the volume phase transition temperature T_c. For the PNIPAM-*co*-allylamine microgels, T_c is ~35 °C, about 1 °C higher than that of PINIPAM particles. This is understandable because the amino group is hydrophilic at neutral pH, independent of temperature. Incorporation of 10 mol % of amino group makes the gel particles more hydrophilic and the phase transition to a higher temperature.

Static light scattering was carried out for PNIPAM-*co*-allylamine microgel (batch 2) dilute dispersions with polymer concentrations ranging from 2.5×10^{-6} to 1×10^{-5} g/mL. Parts a and b of Figure 2 show the Zimm plots at 23 and 35 °C, respectively. From the extrapolation of $KC/R_{vv}(q)$ in eq 1 to the zero angle and zero concentration, the second virial

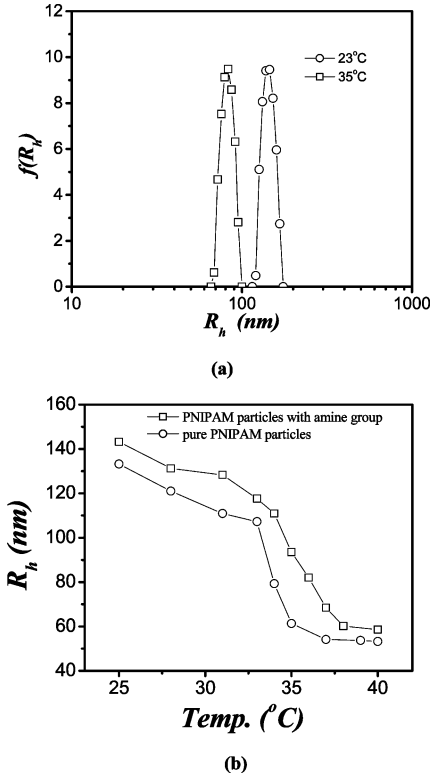

Figure 1. (a) Hydrodynamic radius distributions ($f(R_h)$) of PNIPAM-*co*-allylamine microgels with cross-linking density of 2.5 mol % in water at 23 and 35 °C, respectively. The light scattering angle is 60°. (b) Temperature-dependent hydrodynamic radii of PNIPAM-*co*-allylamine and PNIPAM microgels in water.

coefficient A_2 and the radius of gyration $\langle R_g \rangle$ were obtained. The d*n*/d*C* value was taken as 0.166 cm^3/g for PNIPAM microgels, measured by a refractometer.[30] As shown in Table 2, the positive A_2 at 23 °C shows that water is a good solvent for the PNIPAM-*co*-allylamine at this temperature, while the negative A_2 at 35 °C shows that water becomes poor when the temperature is above the LCST. By combining dynamic and static light scattering results, we obtained that $R_g/R_h = 0.713$ at 23 °C, while at 35 °C, $R_g/R_h = 0.747$, which is close to the theoretical value of $(3/5)^{1/2}$ for the uniform hard spheres. The light scattering properties of PNIPAM-*co*-allylamine microgels are similar to those of PNIPAM microgels.[8,12,31]

2. Phase Behavior of PNIPAM-*co*-allylamine Microgels. The phase behavior of PNIPAM-*co*-allyamine microgel dispersions with various cross-linking densities can be readily observed, as shown in Figure 3 at room temperature. For cross-linking density of 1.5 mol % (batch 4, Figure 3a), crystallization occurs in polymer concentrations ranging between 1.3 and 2.3 wt %. In this range, microgel spheres not only have sufficient interactions but also have enough freedom to form large colloidal crystals. These crystals are easy to observe because of their iridescent domains. Below 1.3 wt %, the microgels randomly diffuse in water and scatter light strongly, resulting in cloudy appearance. On the other hand, above 2.3 wt %, the microgel spheres are no longer free to move around so that a glass phase is formed. In this high concentration range, the dispersions look homogeneous. These observed phase behavior for PNIPAM-*co*-allylamine microgels are similar to pure PNIPAM microgel systems.[8,12]

The formation of colloidal crystals of PNIPAM-*co*-allylamine microgels is dependent not only on polymer concentration but also on cross-linking density. As cross-linking density increases,

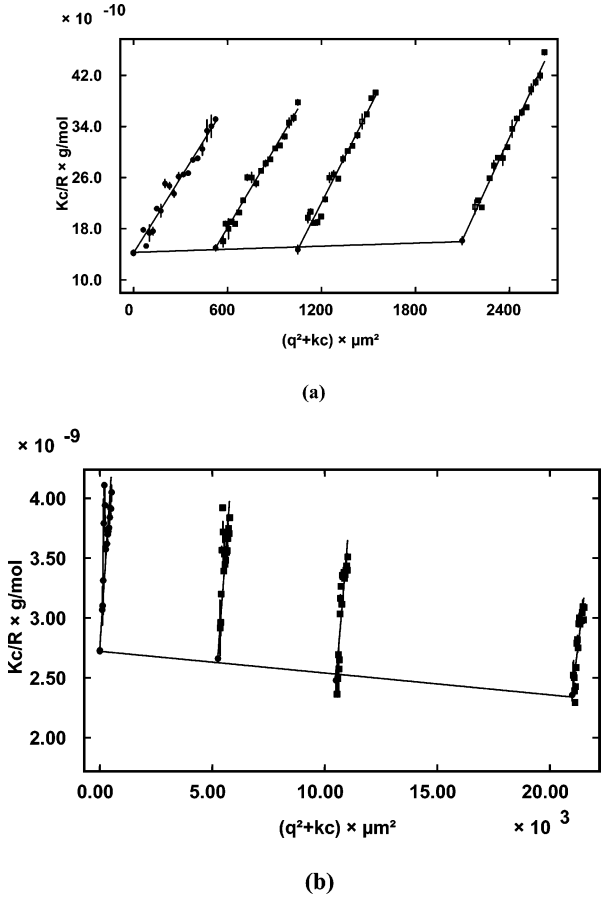

Figure 2. Zimm plots of PNIPAM-*co*-allylamine microgels with cross-linking density of 2.5 mol % at 23 °C (a) and 35 °C (b), respectively. The microgels are dispersed in water with polymer concentrations ranging from right to left: 1.0×10^{-5}, 5.0×10^{-6}, 2.5×10^{-6}, and 0 (extrapolated) g/g.

Table 2. Static and Dynamic Light Scattering Results of the PNIPAM-*co*-allylamine Microgels with 2.5 mol % Cross-Linking Density in an Aqueous Dispersion

temp (°C)	R_h (nm)	R_g (nm)	A_2 (mol dm^3/g^2)	M_w (g/mol)
23	123	87.8	1.425×10^{-8}	3.542×10^8
35	70.3	52.6	-2.34×10^{-8}	3.213×10^8

the formation of colloidal crystals occurs at higher concentrations. The polymer concentration range for crystallization for microgels with cross-linking density of 1.5 mol % is between 1.3 and 2.3 wt % (Figure 3a) but increases to between 2.0 and 3.5 wt % with cross-linking density of 2.5 mol % (batch 5, Figure 3b) and to between 3.3 and 5.0 wt % with cross-linking density of 3 mol % (batch 1, Figure 3c). The temperature of samples in Figure 3b was about 2 °C higher than samples in Figure 3a,c due to two different measurements. This difference had no significant influence in the phase behavior.

Figure 4 summarizes the phase behavior of the PNIPAM-*co*-allylamine microgel dispersions as a function of temperature, polymer concentration, and cross-linking density. Here T_c (dashed line) is the volume phase transition temperature of PNIPAM-*co*-allylamine particles. T_m (open circles) and T_g (open squares) are the melting and glass transition temperature, respectively. T_m (solid circles[24]) and T_g (solid squares) of microgels of batch 5 are also shown in Figure 4b, and they are similar to those of microgels of batch 2. Both batches have the same crosslinking density but slightly different particle sizes. It is noted that the glass transition temperature here means that below this temperature the microgels lost freedom of the

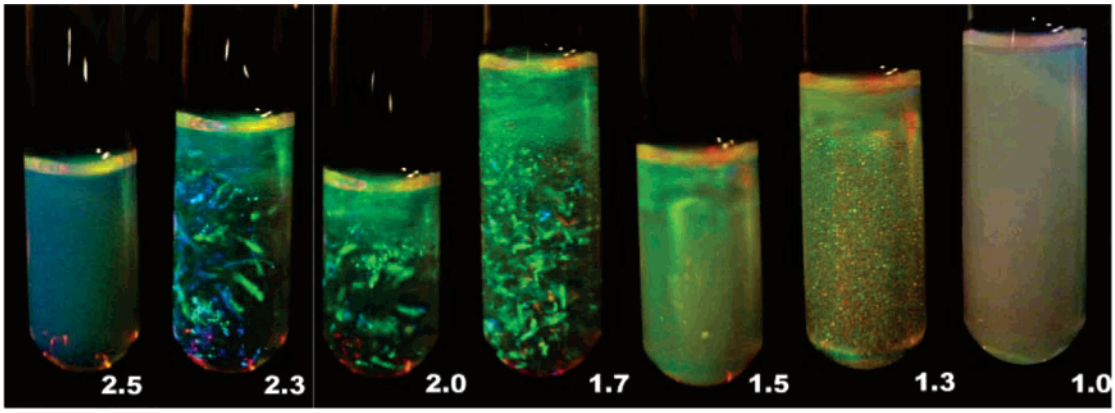

(a)

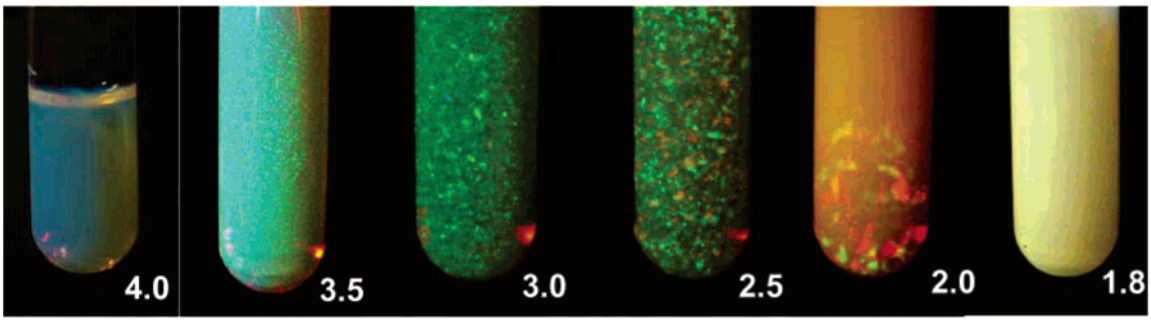

(b)

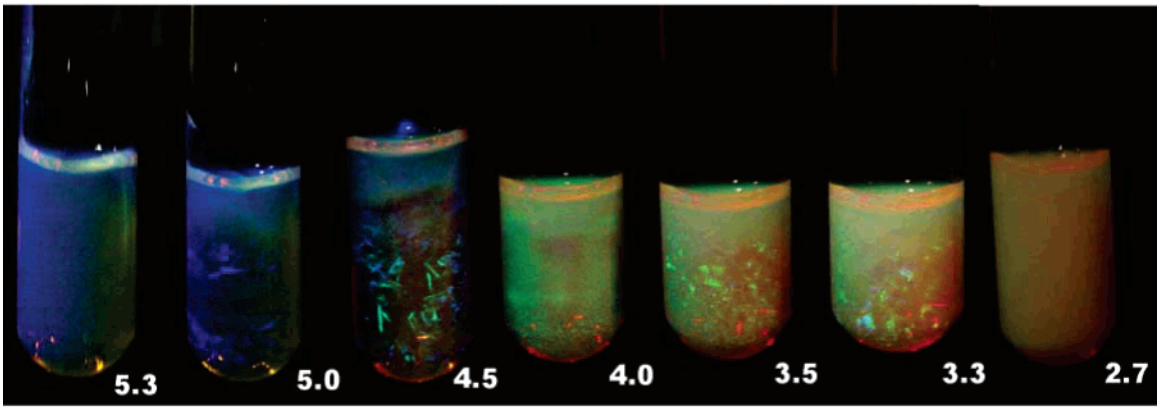

(c)

Figure 3. Photographs of PNIPAM-*co*-allylamine microgel dispersions with different cross-linking densities. (a) Bis/NIPAM = 1.5 mol % at 21 °C. The polymer concentrations are 2.5, 2.3, 2.0, 1.7, 1.5, 1.3, and 1.0 wt % from left to right. (b) Bis/NIPAM = 2.5 mol % at 23 °C. The polymer concentrations are 2.5, 2.3, 2.0, 1.7, 1.5, 1.3, and 1.0 wt % from left to right. (c) Bis/NIPAM = 3.0 mol % at 21 °C. The polymer concentrations are 5.3, 5.0, 4.5, 4.0, 3.5, 3.3, and 2.7 wt % from left to right.

movement and cannot reach their crystalline positions. This is different from T_g, defined in general polymer physics, at which a part of chain in amorphous polymer solid begins micro-Brownian motion.

The phase transition from the liquid to the crystal state across T_m point for PNIPAM−allylamine microgels is similar to pure PINPAM particles dispersed in water.[13b] This transition has been investigated using molecular thermodynamic models assisted with experimental measurements.[13] Using the temperature-dependent size and energy parameters, the Sutherland-like potential provides a reasonable representation of the interparticle potential for PNIPAM particles in swollen and in collapsed phases. The phase diagram calculated from a first-order perturbation theory and an extended cell model indicates that an aqueous dispersion of PNIPAM particles can freeze at both high and low temperatures. At low temperature, the freezing at T_m occurs at large particle volume fraction, similar to that in a hard-sphere system.[13] The phase transition from crystal state to a glass state across T_g for PNIPAM−allyamine is due to swelling of microgels upon the decrease of the temperature. In the glass state, swollen gels compete for surrounding water and lose freedom to move around for the formation of crystals. The close-

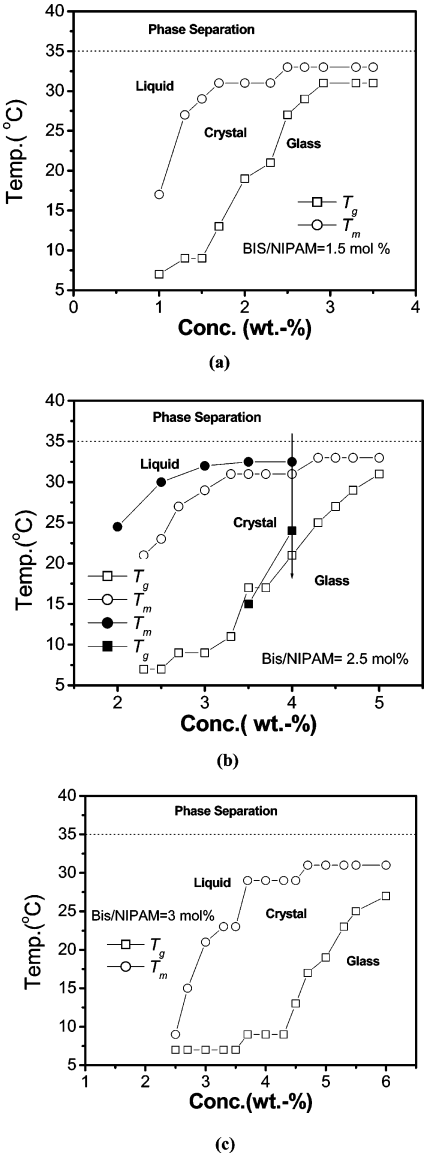

Figure 4. Temperature-dependent phase behavior of the PNIPAM-*co*-allylamine microgel dispersions with different cross-linking densities: (a) Bis/NIPAM = 1.5 mol % (batch 4); (b) Bis/NIPAM = 2.5 mol % (batch 2); (c) Bis/NIPAM = 3.0 mol % (batch 1). The dashed line (T_c) indicates the volume phase transition of the PNIPAM-*co*-allylamine particles. The open circle represents the freezing temperature, T_m, and the open square represents the glass transition temperature, T_g. The solid symbols in Figure 4b are used for microgels of batch 5.

packing of spherical PNIPAM microgels in a concentrated dispersion can lead to a sol−gel transition to form an elastic hybrid gel.[32]

Here we pay an attention to temperature-dependent polymer concentration range that crystallization occurs. With the increase of temperature, crystallization takes place at higher polymer concentration. Microgels of cross-linking density of 1.5 mol % forms crystals between 1.0 and 1.7 wt % at 13 °C. When the temperature increases to 21 °C, the range of crystallization shifts from 1.3 to 2.3 wt %. This concentration increase is expected because the microgels become smaller as the temperature increases (Figure 1b). Thus, more particles are needed to obtain enough interparticle interaction for the formation of crystalline arrays.

Crystallization of microgels starts at effective volume fractions of ca. 0.59 as compared to the freezing transition of 0.494 for hard spheres.[8] With the increasing of the cross-linking

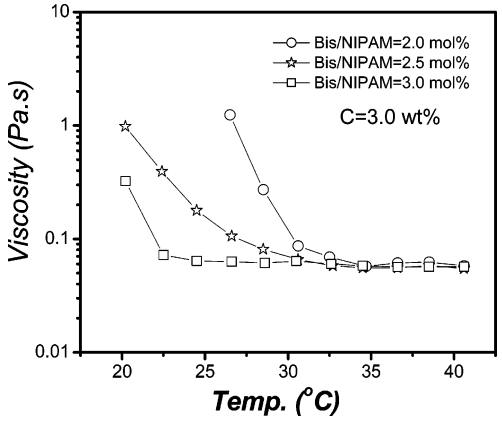

Figure 5. Temperature-dependent viscosity for PNIPAM-*co*-allylamine microgels with different cross-linking densities (batches 3, 2, and 1) in microgel dispersions with polymer concentration of 3 wt %.

density, the subchain length between two neighboring cross-linkers decreases. As a result, a microgel with a low cross-linking density can swell more by absorbing more water than microgels with higher cross-linking density. If both microgels have the same diameter, the microgel with higher cross-linking density is heavier. As a result, the effective volume fractions for crystallization should occur at a high polymer concentration for microgels with higher cross-linking density, as observed in Figure 4.

The effective volume fraction of colloidal dispersions is closely related to its viscosity.[25] Figure 5 shows the viscosity of the PNIPAM-*co*-allylamine microgel dispersions as a function of temperature at three cross-linking densities, measured using a stress-controlled rheometer (ATS Viscoanalyser) with the shear stress about 5 Pa. These samples have the same polymer concentration of about 3 wt %. Viscosity of the microgel with cross-linking density 2 mol % is higher than that of the microgel with higher cross-linking density of 3.0 mol %. This demonstrates that to reach the same polymer concentration, more microgels with low cross-linker density are required than microgels with high cross-linking density. To obtain a proper viscosity so that the microgels have freedom to form crystals, the microgels with lower cross-linking density have to form colloidal crystals at lower polymer concentrations, again, as shown in Figure 4.

The color observed in the dispersions is due to diffraction from ordered colloidal arrays with lattice spacing on the order of the wavelength of visible light. Figure 6a shows UV−vis spectra of the PNIPAM-*co*-allylamine microgel dispersions at various polymer concentrations. These particles have cross-linking density of 2.5 mol % (batch 5). The sharp peak is due to Bragg diffraction and shifts from 640 to 530 nm as the polymer concentration increases from 2.0 to 3.5 wt %. This shift is caused by the decrease in the interparticle distance with increasing polymer concentration. The diffraction wavelength is related to interplane spacing according to the Bragg equation, $m\lambda = 2nd \sin \theta$, where n is the mean refractive index of the dispersion, θ is the diffraction angle, d is the lattice spacing, m is the diffraction order, and λ is the wavelength of diffracted light.[20] Considering polymer concentration in the dispersion as $C = m/V$, the wavelength should be proportional to the $C^{-1/3}$. The value of λ is then plotted as a function of $C^{-1/3}$ as shown in Figure 6b. The solid line in Figure 6b is the best fit to the data with the relationship of $\lambda = -2.51 + 822C^{-1/3}$.

3. Formation of PNIPAM-*co*-allylamine Microgel Hydrogel Opals. The use of PNIPAM colloidal dispersions based on their crystalline structures is limited because the structures can

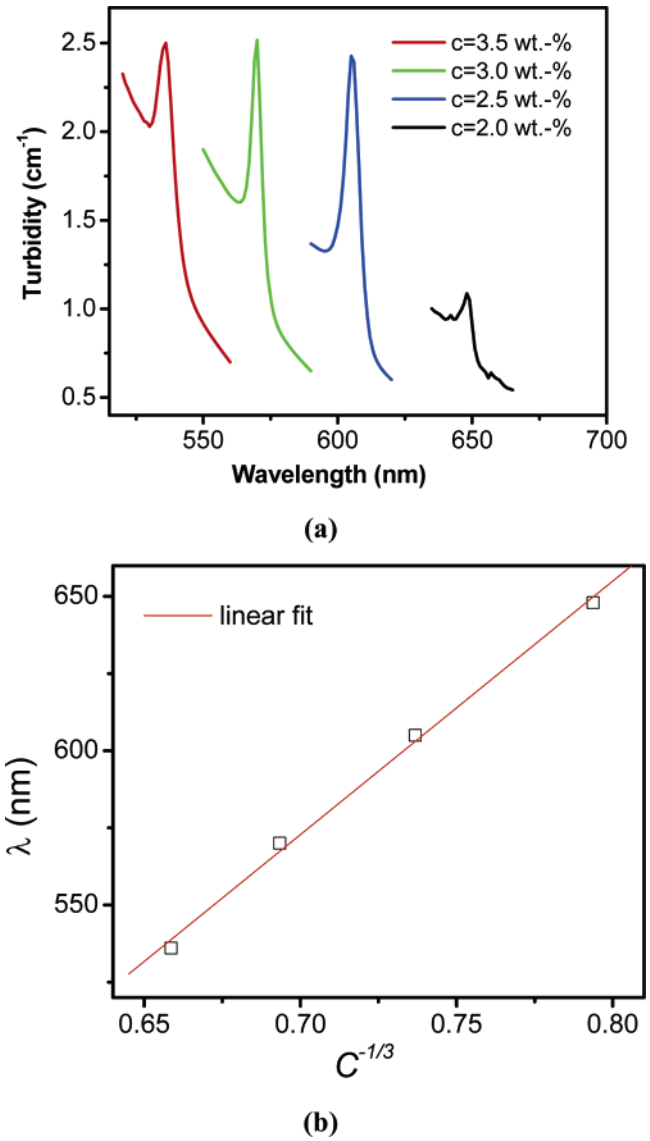

Figure 6. (a) Turbidity vs wavelength curves measured with a UV−vis spectrophotometer. The Bragg diffraction peak shifts to lower wavelengths as the polymer concentration increases. From left to right: 3.5, 3.0, 2.5, and 2.0 wt %. (b) Linear relationship between wavelength of Bragg peak and the concentration of the microgel dispersions. The cross-linking density for these particles (batch 5) is 2.5 mol %.

be easily destroyed by any external disturbance such as small vibrations. The previous approach[23] has a limit that the particles-linking reaction had to be carried out under a harsh environment (pH 12), and the mechanical strength of the bonded particle assembly was weak due to its low polymer concentration. Guided by phase diagrams shown in Figure 4, we have engineered crystalline hydrogels with higher polymer concentrations. We started with a PNIPAM-*co*-allylamine particle (batch 5) dispersion of 4.0 wt % at which the viscosity is too high to allow the particles to form a periodic structure at room temperature. This system was heated from 23 to 40 °C and then cooled back to 23 °C with a rate about 0.4 °C/min. As shown by an arrow in Figure 4b, when the sample was cooled below T_m, the crystallization started. Here the dispersion had low viscosity since the particles were only partially swollen. This allowed the spheres to have enough freedom to self-assemble into an ordered array. The sample was cooled further to below T_g, at which the particle size and viscosity increased considerably. The crystalline structure formed at the higher temperature

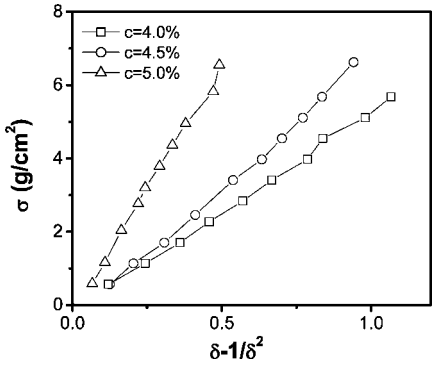

Figure 7. Plot of stress σ vs $(\delta - \delta^{-2})$ for PNIPAM-*co*-allylamine crystalline hydrogels with different polymer concentrations. Here δ is the relative deformation of the sample. The slopes of the best linear fits to the data yield the shear modulus of the sample.

was "frozen" or preserved. Then, the particle assembly with a crystalline structure was fully stabilized by the cross-linking reaction (glutaric dialdehyde) in neutral pH in about 2 days. Because of the higher mechanical strength of this crystalline hydrogel, it is easy to remove from the test tube.

The mechanical properties of these nanostructured hydrogels have been studied from uniaxial compression measurements.[33] The elastic shear modulus G was determined from the slope of linear dependence

$$\sigma = f/S_0 = G(\delta - 1/\delta^2) \quad (5)$$

where f is the value of the exerted force, S_0 is the cross section of the undeformed swollen hydrogels, and δ is the relative deformation of the specimen. Figure 7 shows the shear moduli of the crystalline hydrogels with different polymer concentrations. These hydrogels consist of the same micorgels with cross-linking density (batch 5) of 2.5 mol %. When the concentrations of the crystal hydrogels increases from 4.0 to 5.0 wt. %, the shear modulus increases from 0.53×10^4 to 1.32×10^4 dyn/cm^2. It is apparent that combination between the covalent bonding process and the heating−cooling process can significantly improve the mechanical strength of a crystalline hydrogel.

4. Environmental Responses of PNIPAM-*co*-allylamine Hydrogel Opals. Creating crystalline hydrogels allows us to obtain useful functionalities not only from the periodic structure but also from the constituent building blocks. Because the building blocks here are environmentally responsive colloidal spheres, their sizes as well as the lattice spacing should be tunable by external stimuli. As shown in Figure 8a, the crystalline hydrogel at room temperature displays a bright green color. With the increase of the temperature, the color of the gel changes from green to blue at 31 °C and eventually to milky white at 35 °C, just at the volume phase transition temperature of the particles. When the temperature is decreased to room temperature again, the gel restored its color and volume. This process is fully reversible.

It has been already established that colors of microgel dispersions are related to the Bragg diffraction from periodic arrays of microgels, which is shown as a peak in the UV−vis spectrum in Figure 8b. It is noted as the temperature increases from room temperature, the wavelength of the peak does not change significantly and completely disappears above the melting temperature. In contrast, for a crystalline hydrogel consisting of a cross-linked microgels array, the wavelength of the Bragg peak decreases from about 580 to 520 nm upon the increase of the temperature from 19 to 31 °C (Figure 8c). The change of the peak wavelength is due to the shrinkage of particle

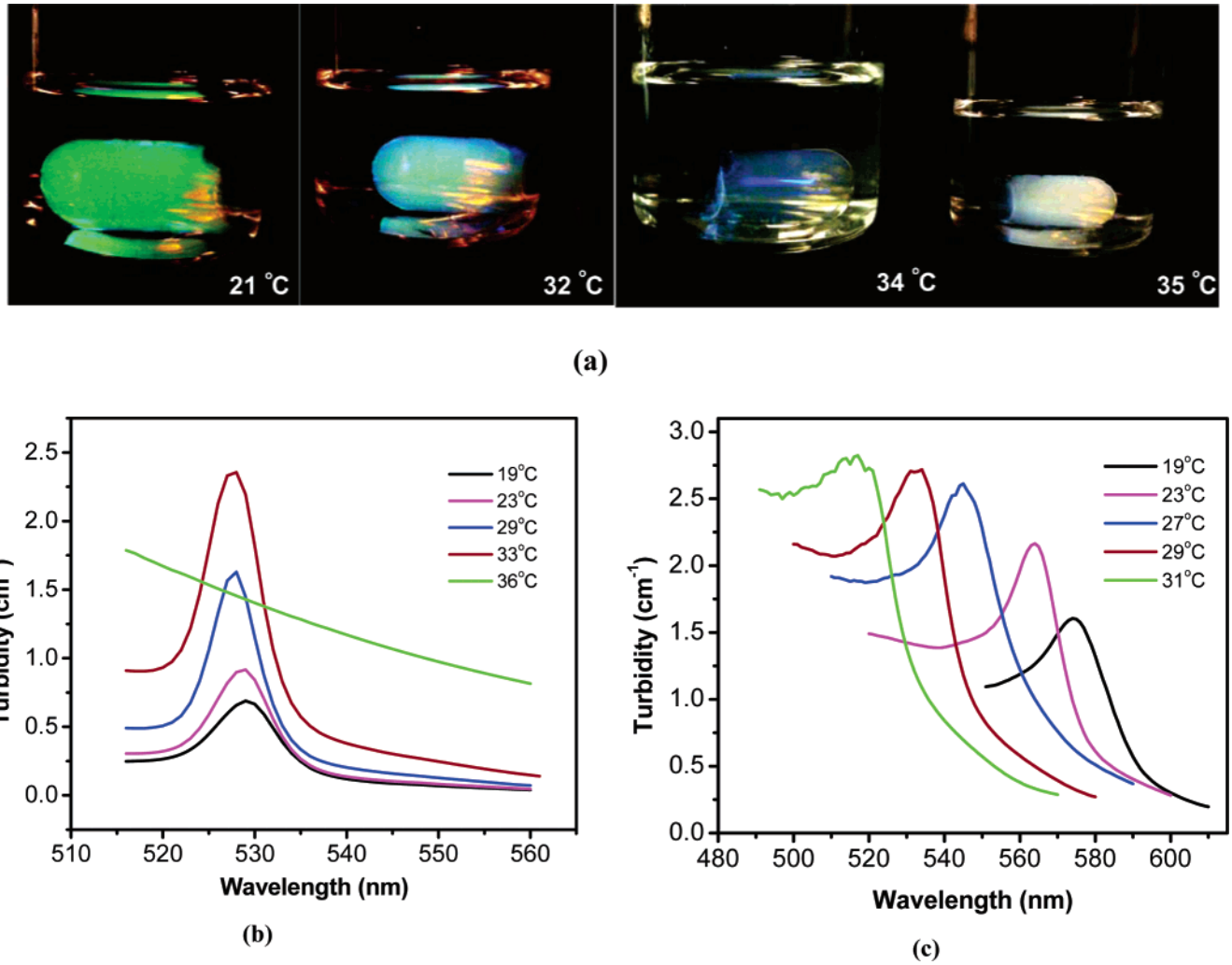

Figure 8. (a) PNIPAM-*co*-allylamine crystal hydrogels switching colors with the change of the temperatures. From left to right, the temperatures are 21, 32, 34, and 35 °C. The turbidity vs wavelength curves measured using a UV−vis spectrophotometer. (b) PNIPAM-*co*-allylamine microgel dispersion with the concentration 4.5 wt. %. (c) PNIPAM-*co*-allylamine crystal hydrogels with the concentration of 4.5 wt %.

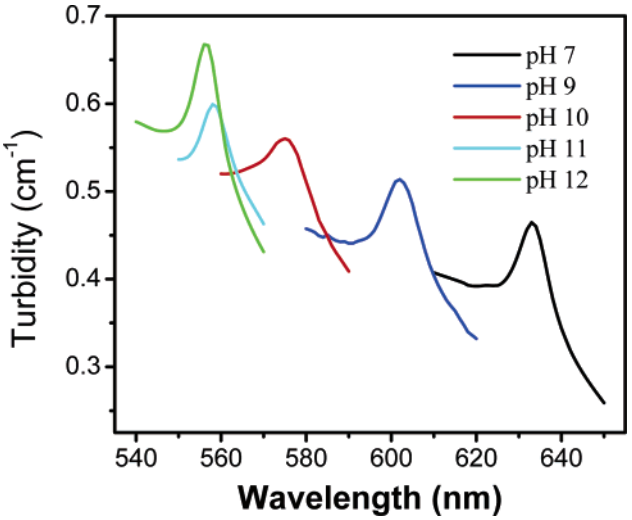

Figure 9. UV−vis spectra of PNIPAM-*co*-allylamine crystal hydrogels as a function of pH value.

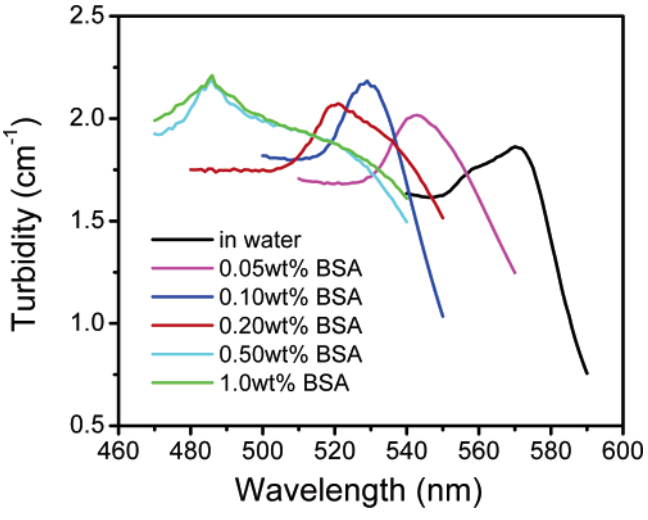

Figure 10. UV−vis spectra of PNIPAM-*co*-allylamine crystal hydrogels as a function of BSA concentration.

size with the temperature, which causes the decrease of interparticle spacing in crystalline hydrogels. In contrast, for a microgel dispersion, the neighboring microgels are not cross-linked. The temperature induced shrinkage of the microgels cannot cause the change of interparticle distance.

Because of residues of basic (i.e., $-NH_2$) groups on the PNIPAM-*co*-allylamine microgels, the swelling capacity of the resulting hydrogel can be changed by controlling the pH value of the medium. The amine groups on the particles are partially ionized in water at a neutral pH, causing swelling of the

particles. At a higher pH, the ionization of the basic groups is inhibited, causing the shrinkage of the particles. This shrinkage of the building block size at higher pH values causes the lattice spacing to decrease, resulting in the color change. The color shift is determined by UV−vis spectroscopy shown in Figure 9. When the pH value changes from 7 to 12, the wavelength of Bragg peak for the hydrogel decreases from 633 to 556 nm. This change of the Bragg peak is especially useful and convenient for monitoring the base environment.

The colors of crystalline hydrogels can also be changed with the change of protein concentration. Here we use bovine serum albumin (BSA) solution to demonstrate this point. As shown in Figure 10, when the concentration of the BSA solution changes from 0 to 1 wt %, the Bragg peak shifts to from 570 to 486 nm. This change is due to the ionic group on BSA, which competes for hydrogen bonding between the microgels and water. This causes the shrinkage of the particles in the network. As the interparticle distance becomes smaller, the color of the hydrogel changes from green to blue as BSA concentration increases.

Conclusion

Monodispersed copolymer *N*-isopropylacrylamide and allylamine (PNIPAM-*co*-allylamine) colloidal spheres with various cross-linking densities have been synthesized using precipitation polymerization. The phase behavior of dispersions of these microgels has been investigated as functions of polymer concentration, temperature, and cross-linking density. It has been found that such microgel dispersions exhibit liquid, crystal, and glass phases. The formation of colloidal crystals of PNIPAM-*co*-allylamine is not only dependent on polymer concentration but also dependent on cross-linking density and temperature. As cross-linking density increases, the formation of colloidal crystals occurs at higher concentrations. At about 21 °C, polymer concentration range for crystallization at cross-linking density of 1.5 mol % is between 1.3 and 2.3 wt % but increases to 2−5.3 wt % for microgels with cross-linking density of 3 mol %. Temperature-dependent viscosity of microgels has been measured and confirmed that the microgels with lower cross-linking density should form colloidal crystals at lower polymer concentrations.

Following the phase diagram, the microgel dispersion with high polymer concentration around 4% was heated from 23 to 40 °C. Then when the sample was cooled below T_m, the crystallization started. As the sample was cooled further to below T_g, the crystalline structure formed at the higher temperature was "frozen". This crystalline structure was fully stabilized by covalently linking neighboring microgels using glutaric dialdehyde in neutral pH. The hydrogel with a higher polymer concentration have a better mechanical strength, while a mild synthesis condition at pH 7 makes this material particularly useful for biomedical applications, including loading biomolecules between the particles for controlled drug delivery.[34] The assembly of interlinked microgels has been taken out from the test tube and measured to obtain the relationship between force and deformation. It is found that the shear modulus of such a crystalline hydrogel is about 0.53×10^4 dyn/cm^2 for the hydrogel opal with a polymer concentration of 4.0 wt %. UV−vis spectroscopy has been used to monitor the change of the Bragg diffraction form these hydrogels as a function of temperature, pH, and protein concentration. The wavelength of the Bragg peak decreases from about 580 to 520 nm upon the increase of the temperature from 19 to 31 °C. The change of the peak wavelength is due to the shrinkage of the particle size with the temperature, which causes the decrease of interparticle spacing in crystalline hydrogels. In contrast, for a microgel dispersion, temperature-induced shrinkage of the microgels cannot cause the change of Bragg diffraction wavelength. When the pH value changes from 7 to 12, the wavelength of Bragg peak for the hydrogel decreases from 633 to 556 nm. A similar wavelength shift has been also observed in bovine serum albumin (BSA) solution. As a result, the crystalline hydrogel may serve as an optical sensor to visually inspect environmental changes.

Acknowledgment. We gratefully acknowledge the support from the National Science Foundation under Grant DMR-0507208.

References and Notes

(1) Tanaka, T. *Phys. Rev. Lett.* **1978**, *40*, 820.
(2) Tanaka, T.; Nishio, I.; Sun, S. T.; Ueno-Nishio, S. *Science* **1982**, *218*, 467.
(3) Peppas, N. A.; Langer, R. *Science* **1994**, *263*, 1715.
(4) Siegel, R. A.; Firestone, B. A. *Macromolecules* **1988**, *21*, 3254.
(5) Hoffman, A. S. *Adv. Drug Delivery Rev.* **2002**, *54*, 3.
(6) Kopecek, J. *Eur. J. Pharmacol. Sci.* **2003**, *20*, 1.
(7) Kim, S. W.; Bae, Y. H.; Okano, T. *Pharm. Res.* **1992**, *9* 283.
(8) Senff, H.; Richtering, W. *J. Chem. Phys.* **1999**, *111*, 1705.
(9) Hellweg, T.; Dewhurst, C. D.; Bruckner, E.; Kratz, K.; Eimer, W. *Colloid Polym. Sci.* **2000**, *278*, 972.
(10) Debord, J. D.; Lyon, L. A. *J. Phys. Chem. B* **2000**, *104*, 6327.
(11) Lyon, L. A.; Debord, J. D.; Debord, S. B.; Jones, C. D.; McGrath, J. G.; Serpe, M. J. *J. Phys. Chem. B* **2004**, *108*, 19099.
(12) Gao, J.; Hu, Z. *Langmuir* **2002**, *18*, 1360.
(13) (a) Wu, J. Z.; Zhou, B.; Hu, Z. B. *Phys. Rev. Lett.* **2003**, *90*, 048304. (b) Wu, J. Z.; Huang, G.; Hu, Z. B. *Macromolecules* **2003**, *36*, 440.
(14) Tsuji, S.; Kawaguchi, H. *Langmuir* **2005**, *21*, 2434.
(15) Alsayed, A. M.; Islam, M. F.; Zhang, J.; Collings, P. J.; Yodh, A. G. *Science* **2005**, *309*, 1207.
(16) Pusey, P. N.; van Megen, W. *Nature (London)* **1986**, *320*, 340.
(17) Liu, J.; Weitz, D. A.; Ackerson, B. J. *Phys. Rev. E* **1993**, *48*, 1106.
(18) Jiang, P.; Bertone, J. F.; Colvin, V. L. *Science* **2001**, *291*, 453.
(19) Xia, Y.; Gates, B.; Yin, Y.; Lu, Y. *Adv. Mater.* **2000**, *12*, 693.
(20) Weissman, J. M.; Sunkara, H. B.; Tse, A. S.; Asher, S. A. *Science* **1996**, *274*, 959. Holtz, J. H.; Asher, S. A. *Nature (London)* **1997**, *389*, 829.
(21) Lee, Y.; Braun, P. V. *Adv. Mater.* **2003**, *15*, 563.
(22) Nakayama, D.; Takeoka, Y.; Watanabe, M.; Kataoka, K. *Angew. Chem., Int. Ed.* **2003**, *42*, 4197.
(23) Hu, Z. B.; Lu, X. H.; Gao, J.; Wang, C. J. *Adv. Mater.* **2000**, *12*, 1173. Hu, Z. B.; Lu, X. H.; Gao, J. *Adv. Mater.* **2001**, *13*, 1708.
(24) Hu, Z.; Huang, G. *Angew. Chem., Int. Ed.* **2003**, *42*, 4799.
(25) Senff, H.; Richtering, W. *Colloid Polym. Sci.* **2000**, *278*, 830.
(26) Debord, J. D.; Eustis, S.; Debord, S. B.; Lofye, M. T.; Lyon, L. A. *Adv. Mater.* **2002**, *14*, 658.
(27) Pelton, R. H.; Chibante, P. *Colloids Surf.* **1986**, *20*, 247.
(28) Chu, B. *Laser Light Scattering*, 2nd ed.; Academic Press: New York, 1991.
(29) Berne, B. J.; Pecora, R. *Dynamic Light Scattering*; Wiley: New York, 1976.
(30) Xia, X. H.; Hu, Z. B. *Langmuir* **2004**, *20*, 2094.
(31) Wu, C.; Zhou, S. Q.; Auyeung, S. C. F.; Jiang, S. H. *Angew. Makromol. Chem.* **1996**, *240*, 123.
(32) Zhao, Y.; Cao, Y.; Yang, Y.; Wu, C. *Macromolecules* **2003**, *36*, 855.
(33) Gehrke, S. H. *Adv. Polym. Sci.* **1993**, *110*, 81.
(34) Huang, G.; Gao, J.; Hu, Z. B.; John, J. V.; Ponder, B. C.; Moro, D. *J. Controlled Release* **2004**, *94*, 303.

MA070253D